Lawrence Berkeley National Laboratory
LBL Publications

Title

Modeling Synergistic Fuel Cell Membrane Degradation with Mitigating Effects of Cerium

Permalink

Journal

ISSN

Authors

Ehlinger, Victoria Marie
Kusoglu, Ahmet
Weber, Adam Z

Publication Date

DOI

Peer reviewed

PAPER • OPEN ACCESS

Modeling proton-exchange-membrane fuel cell performance/degradation tradeoffs with chemical scavengers

To cite this article: Victoria M Ehlinger *et al* 2020 *J. Phys. Energy* **2** 044006

View the article online for updates and enhancements.

You may also like

- Structures and Free Energies of Cerium Ions in Acidic Electrolytes and Structures of Electrolyte-Electrode Interfaces to Inform Kinetic Performance in Redox Flow Battery Applications
Cailin Buchanan, Eunbyeol Ko, Bryan R. Goldsmith et al.

- Cerium Migration during PEM Fuel Cell Assembly and Operation
Andrew M Baker, Dennis Torraco, Elizabeth J. Judge et al.

- Possible Repair Mechanism for Hydrocarbon-Based Ionomers Following Damage by Radical Attack
Tym de Wild, Tamas Nemeth, Tom M. Nolte et al.

Recent citations

- Understanding Multi-Ion Transport Mechanisms in Bipolar Membranes
Justin C. Bui *et al*

Journal of Physics: Energy

PAPER

Modeling proton-exchange-membrane fuel cell performance/degradation tradeoffs with chemical scavengers

Victoria M Ehlinger[1,2] , Andrew R Crothers[1,2] , Ahmet Kusoglu[2] and Adam Z Weber[2,3]

1 Department of Chemical and Biomolecular Engineering, University of California, Berkeley, CA 94720, United States of America
2 Energy Technologies Area, Lawrence Berkeley National Laboratory (LBNL), Berkeley, CA 94720, United States of America

E-mail: azweber@lbl.gov

Abstract

One of the primary limiting factors for proton-exchange-membrane (PEM) fuel-cell lifetime is membrane degradation driven by operational stressors such as generation of highly reactive radical species, which result in cell failure and voltage decay. To extend the lifetime of the membrane, cerium ions are added to the membrane to mitigate the effects of chemical degradation by scavenging radicals produced by crossover of reactant gases across the PEM. Although cerium has shown to be very effective at reducing chemical degradation during PEM fuel cell operation, the cerium ions also lead to a decrease in performance due to changes in the membrane transport properties and possible site blockage in the catalyst layers. In this paper, a full-cell, transient performance and durability model is presented in which a micro-kinetic framework accounts for gas crossover induced degradation and concentrated-solution theory describes transport in the PEM. The transport model takes into account the coupled nature of the electrochemical driving forces that cause transport of cerium ions, protons, and water. The cell model predicts the migration of cerium out of the membrane and into the catalyst layers and its impact on performance. A comparison between dilute-solution-theory and concentrated-solution-theory models shows how water management in the cell also effects cerium distribution, where higher relative humidity leads to better retention of cerium in the membrane. A voltage loss breakdown shows that cerium leads to performance losses in the cell both by decreasing proton activity and by modifying transport properties of water and protons through the membrane. Transient simulations show that the optimal tradeoff between performance and durability metrics is reached at low cerium concentrations in the membrane (less than 1% of membrane sulfonic acid sites occupied by cerium for our analysis). Finally, analysis of membrane thickness and catalyst layer thickness as design parameters shows that thicker membranes and thinner catalyst layers best optimize both performance and durability.

Nomenclature

Roman

a_i	activity of species i
c_i	concentration of species i (mol cm^{-3})
D_i	diffusivity of species i (cm^2 s^{-1})
D_{ij}	binary diffusion coefficient for species i and (cm^2 s^{-1})

3 Author to whom any correspondence should be addressed.

E_h	effectiveness factor of reaction h
F	Faraday's constant (96 485 C equiv^{-1})
f_{ce}	fraction of sulfonic acid sites occupied by cerium
f	membrane water fraction
i_h	current density of reaction h (A cm^{-2})
K_{ij}	friction factor for species i and j
k_h	rate constant of reaction h
$\mathbf{N}_i$	flux of species i (mol cm^{-2} s^{-1})
n_i	total moles of species i (mol)
n_h	number of electrons in reaction h
p_i	partial pressure of species i (bar)
p_i^{ref}	reference pressure for species i (1 bar)
p	total pressure (bar)
r_h	rate of reaction h
R	ideal gas constant (8.314 J mol^{-1} K^{-1})
R_i	reaction rate of species i
T	temperature (K)
t_i	transference number of species i
U_0^h	equilibrium potential of reaction h(V)
u_i	ionic mobility of species i (cm^2 V^{-1} s^{-1})
v_i	velocity of species i (cm s^{-1})
z_i	valence of species i

Greek

α_{ij}	transport coefficient for species i and j (mol^2 J^{-1} cm^{-1} s^{-1})
α_a	anode transfer coefficient
α_c	cathode transfer coefficient
η	viscosity (Pa·s)
κ	conductivity (S cm^{-1})
λ	water content
μ_i	(electro)chemical potential of species i (J mol^{-1})
$\mu_{i,n}$	electrochemical potential of species i relative to that of species n (J mol^{-1})
ν_i	stoichiometric coefficient of species i
ξ	electro-osmotic coefficient
ρ_i	density of species i (mol cm^{-3})
Φ	potential (V)
ψ_i	permeability of species i (mol bar^{-1} cm^{-1} s^{-1})

Superscripts and subscripts

0	initial value
1	electron-conducting phase
2	proton-conducting phase
a	anode
c	cathode
Ce	cerium
H	protons
M	membrane
ref	reference
SO_3^-	sulfonic acid groups in the membrane
w	water

Vectors and arrays

D	vector of driving forces
L^M	matrix of inverted friction coefficients
M^M	transport coefficient matrix
V	vector of velocities

Abbreviations

EW	equivalent weight
FRR	fluoride release rate
GDL	gas diffusion layer
HOR	hydrogen oxidation reaction
MEA	membrane electrode assembly
OCV	open circuit voltage
ORR	oxygen reduction reaction
PEM	proton-exchange membrane
PFSA	perfluorosulfonic acid
RH	relative humidity

1. Introduction

With increasing interest in proton-exchange-membrane fuel cells (PEMFCs) for medium- and heavy-duty applications, the research needs shift towards improving lifetime and durability to enable commercialization. During PEMFC operation, a combination of mechanical and chemical stressors occur that lead to loss of performance, or even failure of the proton-exchange-membrane (PEM). Failure could occur in the form of formation and growth of defects, delamination, membrane thinning, etc [1–5]. Chemical degradation results from the oxidative attack of hydroxyl radicals to the chemical bonds in the ionomer's fluorocarbon backbone and side-chains [6–8]. Such radicals are generated by the decomposition of H_2O_2, which can be formed electrochemically or when reactant gases cross through the membrane [1, 9, 10]. Hydroxyl radicals are also generated via Fenton's reaction of H_2O_2 with iron ions, which is believed to be present in the PEM due to migration from the metallic bipolar plates [11, 12]. Mechanical degradation typically occurs due to stresses acting on manufacturing defects in the membrane or sites initiated by chemical attack during operation [1, 3, 4, 13–17].

To reduce chemical degradation in PEMFCs, radical scavengers are embedded into the membrane. The purpose of these radical scavengers is to react with the hydroxide radicals before attacking the membrane due to more favorable thermodynamics and faster reaction kinetics. Experiments have shown that cerium acts as a highly effective mitigant of membrane degradation in PEMFCs [18–20]. However, increasing concentrations of cerium in the PEM decrease its proton conductivity and inhibit the oxygen-reduction-reaction kinetics due to a lower availability of protons, which can result in proton limiting currents [5, 21–24]. Modeling studies have shown the tradeoffs for durability and performance due to varying cerium content in PEMs [25–27]. Previous work showed the coupled nature of mechanical and chemical degradation by incorporating membrane degradation and pinhole effects into the PEM fuel-cell performance model [28]. Here, a microkinetic model for chemical degradation is incorporated along with the mitigating effects of cerium. A concentrated-solution-theory model is used to model the transport of cerium through the membrane and catalyst layers. This approach allows important consideration of the effects of cerium on water and proton transport and identifies two phenomena that cause performance losses when cerium is added to the fuel-cell membrane.

The outline of this paper is as follows. First, the model approach is described, including concentrated-solution-theory approach for cerium transport, the effect of cerium on reaction kinetics, and chemical degradation and mitigation kinetics. A comparison between the concentrated-solution-theory based model and dilute-solution theory model is then carried out. Next, a voltage-loss breakdown elucidates the contributions of cerium to performance losses in the PEMFC. Finally, a study of the trade-offs between performance and durability is accomplished along with a sensitivity analysis with respect to membrane thickness.

2. Theoretical

A diagram of the modeling domain and location of key degradation species is shown in figure 1. The model presented here builds upon our previous model, which is transient, one-dimensional across the PEMFC sandwich (includes the gas diffusion layers (GDLs), catalyst layers, (CLs) and membrane), and assumes water is present in the vapor-phase only (i.e. lower RH feeds) [28]. A mass and energy balance on the gas channels is carried out and used as the boundary conditions for temperature and water flux in the cell. It is assumed that current flows through two phases: an electron-conducting solid phase and the proton-conducting membrane phase. In the gas-transporting GDL and porous CL, the model uses multicomponent diffusion Stefan-Maxwell equations. In the CL, an agglomerate model accounts for the transport of gases to the platinum catalyst sites. Ohm's law describes current in the electron-conducting phases of the GDL and CL.
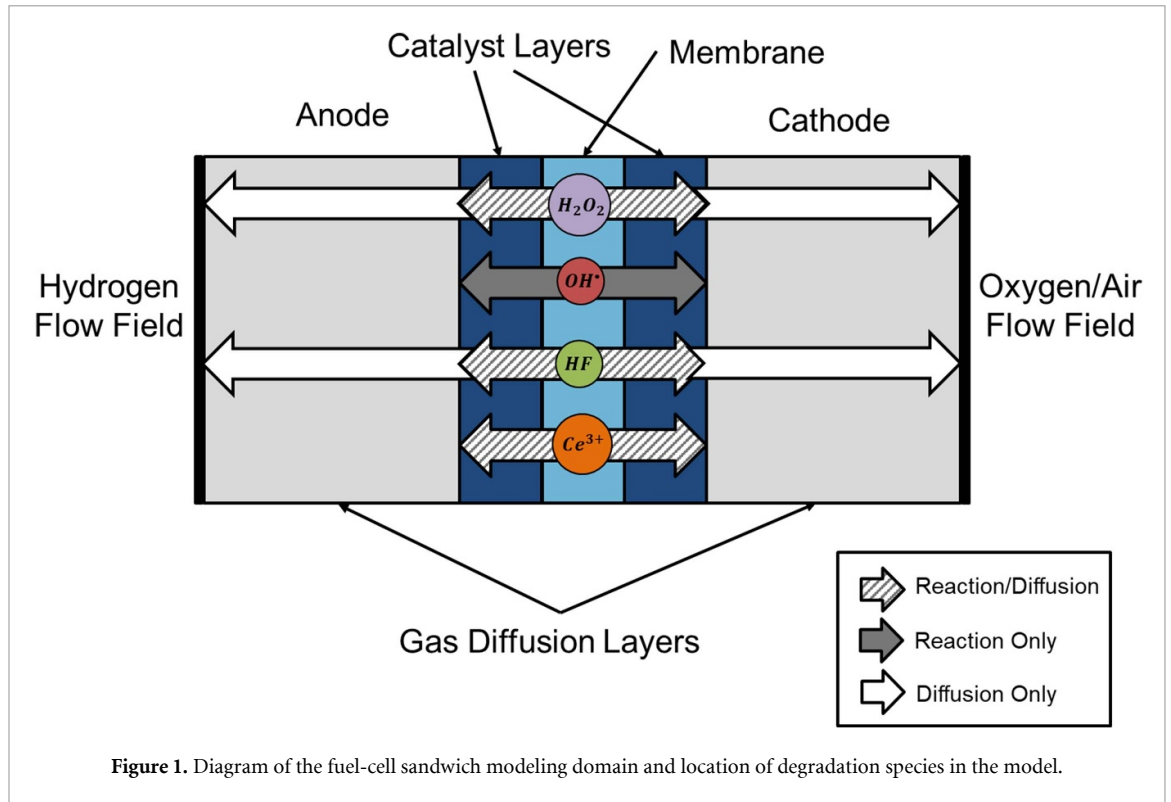
Figure 1. Diagram of the fuel-cell sandwich modeling domain and location of degradation species in the model.

Table 1. Physical properties.

Property		Units	Equation	Ref
Water density	ρ_w	g cm^{-3}	$1.1603 - 5.371 \times 10^{-4}T$	[29]
Water viscosity	μ_w	bar·s	$1 \times 10^{-11}(2695.3 - 6.6T)$	[29]
Water vapor pressure	p_w^{vap}	bar	$\exp\left(11.6832 - \frac{3816.44}{T-46.13}\right)$	[29]
Hydrogen/water diffusion coefficient	$p\mathcal{D}_{H_2,w}$	bar·cm^2 s^{-1}	$2.470\left(\frac{T}{146.55}\right)^{2.334}$	[29]
Oxygen/water diffusion coefficient	$p\mathcal{D}_{O_2,w}$	bar·cm^2 s^{-1}	$0.3022\left(\frac{T}{323.83}\right)^{2.334}$	[30]
Nitrogen/oxygen diffusion coefficient	$p\mathcal{D}_{N_2,O_2}$	bar·cm^2 s^{-1}	$0.0544\left(\frac{T}{143.01}\right)^{1.823}$	[30]
H_2O_2 diffusion coefficient in the membrane/CLs	$\mathcal{D}_{H_2O_2,M}$	cm^2 s^{-1}	1.5×10^{-6}	[31]
H_2O_2 diffusion coefficient in the GDLs	$\mathcal{D}_{H_2O_2,GDL}$	cm^2 s^{-1}	0.188	[32]
HF diffusion coefficient in the membrane/CLs	$\mathcal{D}_{HF,M}$	cm^2 s^{-1}	1.5×10^{-6}	[31]
HF diffusion coefficient in the GDLs	$\mathcal{D}_{HF,GDL}$	cm^2 s^{-1}	0.26	[32]
Electrode specific interfacial area	a	cm^{-1}	8×10^5	fit
Membrane/water vapor rate constant	k_{M,H_2O}	$\frac{\text{mol}^2}{\text{s·J·cm}^3}$	1000	fit

Physical constants used in the model, including binary diffusion coefficients and membrane properties, are listed in table 1. Noted below are the changes of the traditional and previous governing equations due to inclusion of cerium and chemical degradation kinetics.

2.1 Cerium-ion transport model

The equations describing transport of water and protons through the membrane is derived from concentrated-solution theory, where the membrane acts as the reference velocity (i.e. zero velocity relative to the laboratory frame of reference for negligible swelling rate) [33, 34]. For a multicomponent system that is isothermal and isotropic, transport of all mobile species i obeys,

$$c_i \nabla \mu_i = K_{iM}(-v_i) + \sum_{j \neq i,M} K_{ij}(v_j - v_i) \tag{1}$$

Where c_i, μ_i, and v_i are the concentration, chemical potential, and velocity of species i, respectively, and K_{ij} is the friction coefficient between species i and j, and K_{iM} is the friction coefficient between species i and the

membrane [35]. To satisfy the Gibbs–Duhem equation, for the membrane,

$$c_M \nabla \mu_M - \nabla p = \sum_{i \neq M} K_{iM} v_i \tag{2}$$

Where p is the pressure. This results in $N - 1$ independent equations for a system with N species.

Onsager's reciprocal relations show that $K_{ij} = K_{ji}$, therefore a system with N species will have $\frac{N(N-1)}{2}$ friction coefficients [36]. The friction coefficients are related to the binary diffusion coefficients by,

$$\mathcal{D}_{ij} = \frac{RTc_ic_j}{K_{ij}c_T} \tag{3}$$

Where $\mathcal{D}_{ij}$ is the binary diffusion coefficient of species i and j, R is the ideal gas constant, T is the temperature, c_T is the total molar concentration of the solution [35].

For the system of interest, which is 1D across the PEMFC sandwich, equation (1) in matrix form is

$$D = M^M V \tag{4}$$

Where D is the vector of driving forces with length $N - 1$, V is the vector of velocities with length $N - 1$, and M^M is the transport coefficient matrix with dimensions $N - 1$ by $N - 1$. equation (2) is excluded from the matrix (i.e. it is the Nth equation) because it depends on the $N - 1$ instances of equation (1) The superscript M denotes that the reference velocity is that of the membrane. The entries of the matrix are $D_i = c_i \nabla \mu_i$, $V_i = v_i$, and $M_{ij}^M = K_{ij}$ for $i \neq j$ and $M_{ii}^M = -\sum_{j \neq i} K_{ij}$.

In an isothermal system, inverting equation (4) relates the flux of species i to a linear combination of non-membrane electrochemical potentials,

$$N_i = -\sum_{j \neq M} L_{ij}^M c_i c_j \nabla \mu_j \tag{5}$$

Where c_i is the concentration of species i, $\mathbf{N}_i$ is the molar flux vector of species i, and L_{ij}^M is the transport coefficient for species i and j [33] The matrix L^M with entries L_{ij}^M is symmetric and has dimensions $N - 1$ by $N - 1$, where N is the total number of species in the system (including the membrane). L^M is defined as

$$L^M = -\left(M^M\right)^{-1} \tag{6}$$

The L_{ij}^M transport coefficients are not measured directly because experimental conditions that isolate each of these coefficients are not practical. To use this system of equations, the transport coefficient matrix must be rewritten in terms of measurable properties,

$$\mathbf{N}_i = -\sum_{j \neq M} \left(\alpha_{ij}^M + \frac{t_i^M t_j^M \kappa}{z_i z_j F^2} \right) \nabla \mu_{j,n} - \frac{t_i^M \kappa}{z_i F^2} \frac{\nabla \mu_n}{z_n} \tag{7}$$

Where F is Faraday's constant, z_i is the valance of species i, and $\mu_{i,n} = \mu_i - \frac{z_i}{z_n}\mu_n$ is the chemical of species i relative to charged species n, α_{ij}^M is the transport coefficient for species i and j, t_i^M is the transference number for species i, κ is the ionic conductivity, and ξ is the electroosmotic coefficient [37] α_{ij} is symmetric ($\alpha_{ij} = \alpha_{ji}$) and is similar to a generalized effective diffusion coefficient and describes the flux of i due to a chemical potential gradient of $\mu_{i,n}$ in the absence of current. $\mu_{i,n}$ quantifies the chemical potential of species i and, since it is taken relative to charged species n, is independent of electric potential. μ_n is the only term that depends on the electric potential in the membrane. The relationship between these properties and the entries in L^M are

$$\kappa = F^2 \sum_{i \neq M} \sum_{j \neq M} L_{ij}^M z_i c_i z_j c_j \tag{8}$$

$$t_i^M = \frac{z_i c_i F^2}{\kappa} \sum_{j \neq M} L_{ij}^M z_j c_j \tag{9}$$

$$\xi = \frac{t_w^M}{z_w} \tag{10}$$

$$\alpha_{ij}^M = L_{ij}^M c_i c_j - \frac{t_i^M t_j^M \kappa}{z_i z_j F^2} \tag{11}$$

Note that the electro-osmotic coefficient has a finite value although $z_w = 0$ [37].

Reactions at the electrodes in the PEMFC involve protons and, as such, the electric potential is typically quantified by the electrochemical potential of a proton (i.e. a proton reference electrode). Therefore, a convenient choice for the electrochemical reference species n is the proton, so that $\mu_n = \mu_H = F\Phi$. Using this definition, equation (8) with protons (H) set as the reference species, yields for protons,

$$\mathbf{N}_H = -\left(\alpha_{HCe}^M + \frac{t_H^M t_{Ce}^M \kappa}{z_H z_{Ce} F}\right)\nabla\mu_{Ce,H} - \left(\alpha_{Hw}^M + \xi \frac{t_H^M \kappa}{z_H F}\right)\nabla\mu_w - \frac{t_H^M \kappa}{z_H F}\nabla\Phi \tag{12}$$

for cerium,

$$\mathbf{N}_{Ce} = -\left(\alpha_{CeCe}^M + \left(\frac{t_{Ce}^M}{z_{Ce}}\right)^2 \frac{\kappa}{F}\right)\nabla\mu_{Ce,H} - \left(\alpha_{Cew}^M + \xi \frac{t_{Ce}^M \kappa}{z_{Ce} F}\right)\nabla\mu_w - \frac{t_{Ce}^M \kappa}{z_{Ce} F}\nabla\Phi \tag{13}$$

and for water,

$$\mathbf{N}_w = -\left(\alpha_{wCe}^M + \xi \frac{t_{Ce}^M \kappa}{z_{Ce} F^2}\right)\nabla\mu_{Ce,H} - \left(\alpha_{ww}^M + \xi^2 \frac{\kappa}{F^2}\right)\nabla\mu_w - \xi \frac{\kappa}{F}\nabla\Phi \tag{14}$$

To relate $\mu_{Ce,H}$ to the species concentrations, an ideal solution for cerium, protons and the membrane is assumed,

$$\nabla\mu_{Ce,H} = \frac{RT}{c_{Ce}}\nabla c_{Ce} - \left(\frac{z_{Ce}}{z_H}\right)\frac{RT}{c_H}\nabla c_H \tag{15}$$

The friction factors are calculated using the theory of multi-ion transport developed by Crothers *et al* [38, 39]. which is summarized in the supplemental Material (available online at stacks.iop.org/JPENERGY/2/044006/mmedia) and uses the parameters in table S1. Figure 2 shows the results of these calculations for a range of water content and cerium concentrations, based on the experimental data reported in reference [40].

Using the measured data [40], the dependence of water uptake on the concentration of cerium is calculated using a polynomial fit of cerium content and water activity,
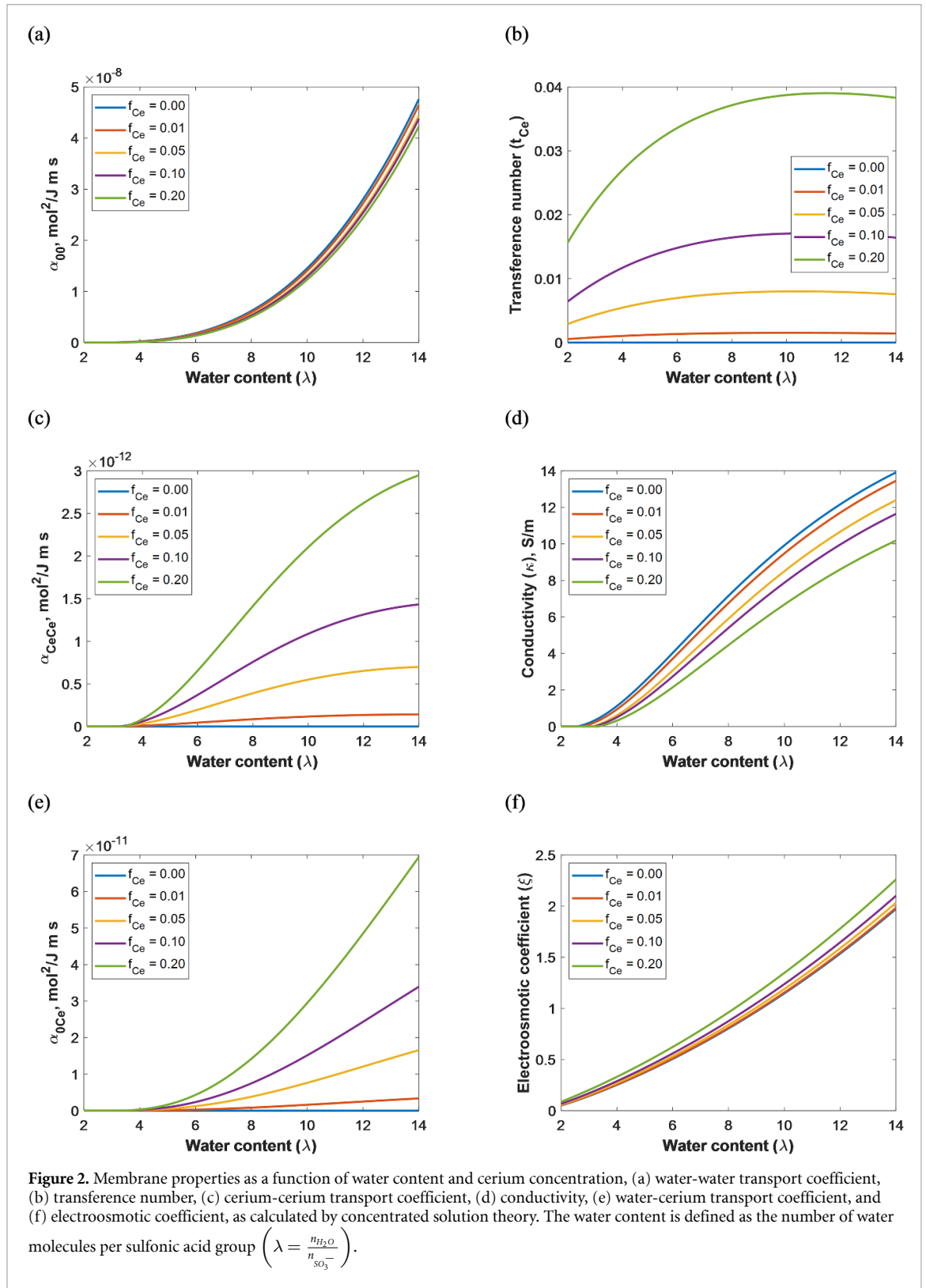
$$\lambda = 1.426 + 9.88a + 0.1256f_{Ce} - 14.73a^2 + 2.826af_{Ce} + 14.42a^3 - 4.0406a^2 f_{Ce} \tag{16}$$

Where λ is the water content, which is defined as the ratio of water molecules to sulfonic acid sites, a is the water activity, and f_{Ce} is the fraction of sulfonic acid sites in the membrane that are occupied by cerium ions,

$$f_{Ce} = \frac{z_{Ce^{3+}} c_{Ce^{3+}}}{\rho_M / EW} \tag{17}$$

Where ρ_M is the membrane density and EW is the equivalent weight of the polymer (1100 g mol^{-1}) [40]. An illustration of cerium in the membrane and how f_{Ce} is calculated is shown in figure 3.
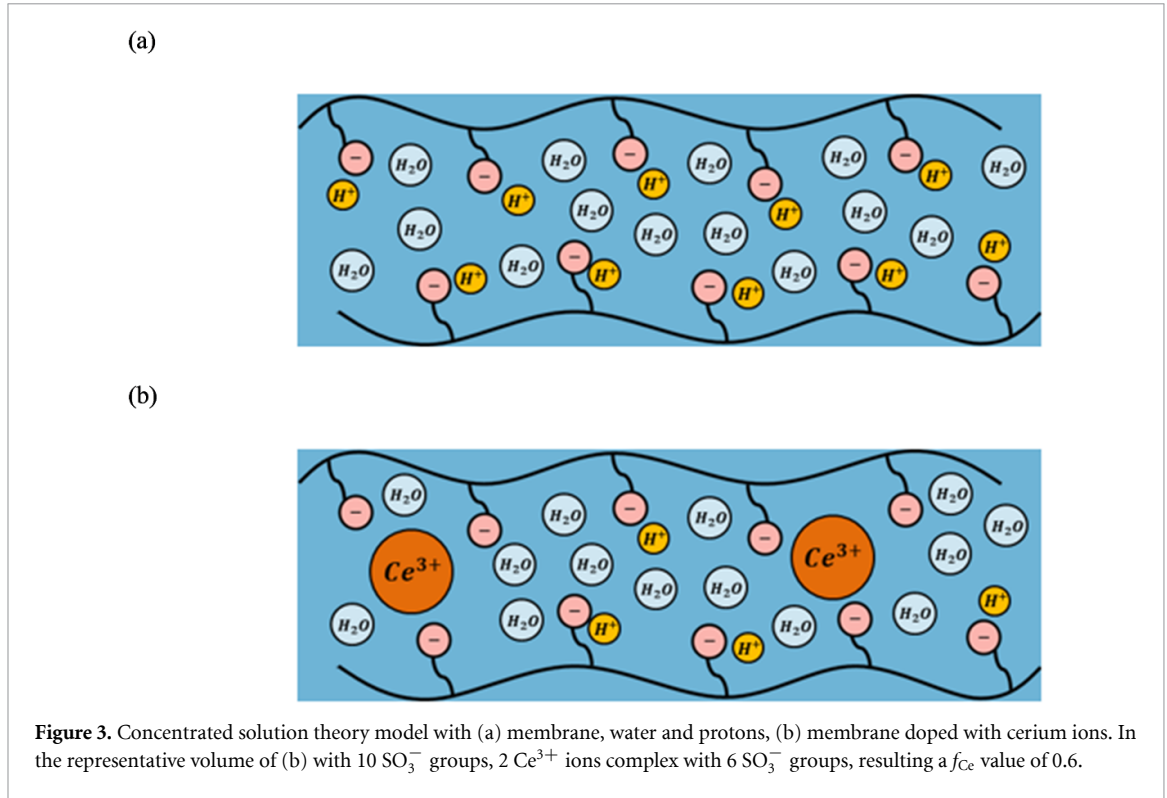
The operating potential for the PEMFC results in a high overpotential for the Ce^{3+}/Ce^{4+} redox reaction ($E^0 = 1.44$ V), driving cerium ions into the $3+$ charge state [25, 27]. Therefore, cerium in the membrane is assumed to be present only in the $3+$ charge state and the concentration of cerium ions in the $4+$ charge state is considered to be equal to approximately zero. A more complete analysis of the Ce^{3+}/Ce^{4+} redox couple in PFSA membranes is analyzed by Gubler and Kopponel, who demonstrated that >99.99% of cerium ions are present in the $3+$ charge state [27]. The model can be extended to include the effects of Ce^{4+}, which may be an important consideration for analysis of start/stop cycles, by modifying the concentrated-solution-theory equations.

Figure 2. Membrane properties as a function of water content and cerium concentration, (a) water-water transport coefficient, (b) transference number, (c) cerium-cerium transport coefficient, (d) conductivity, (e) water-cerium transport coefficient, and (f) electroosmotic coefficient, as calculated by concentrated solution theory. The water content is defined as the number of water molecules per sulfonic acid group $\left(\lambda = \frac{n_{H_2O}}{n_{SO_3^-}} \right)$.

Assuming that the cerium cannot leave the ionomer, an additional mass balance is required to determine the concentration profile within the membrane phase of the PEMFC,

$$\int_0^x c_{Ce} dx = n_{Ce} \tag{18}$$

Where n_{Ce} is the total number of moles of cerium ions initially present in the membrane at the beginning-of-life and x is the distance across the membrane and catalyst layers. This formulation ensures conservation of the mass of cerium inside of the membrane-electrode assembly (MEA). Experiments have

Figure 3. Concentrated solution theory model with (a) membrane, water and protons, (b) membrane doped with cerium ions. In the representative volume of (b) with 10 SO_3^- groups, 2 Ce^{3+} ions complex with 6 SO_3^- groups, resulting a f_{Ce} value of 0.6.

shown the presence on cerium in the PEMFC effluent, indicating that cerium can leave the cell via ion pairing [41]. However, the amount of cerium that exits the cell is very small, on the order of ng cm^{-2}, and is therefore neglected in the model.

2.2 Cerium-ion impact on reaction kinetics

The hydrogen-oxidation reaction (HOR) and the oxygen-reduction reaction (ORR) that predominantly occur at the anode and cathode, respectively, can in reality occur at either electrode due to the crossover of H_2 and O_2 through the membrane. In addition, the two-electron ORR can take place and form hydrogen peroxide. Butler–Volmer kinetics are used for HOR and Tafel kinetics are used for ORRs,

$$i_{HOR} = i_{0_{HOR}} \left[\frac{p_{H_2}}{p_{H_2}^{ref}} \exp\left(\frac{\alpha_a F}{RT} \left(\Phi_1 - \Phi_2 - U_0^{HOR} \right) \right) - \left(\frac{a_{HM}}{a_{HM}^{ref}} \right)^2 \exp\left(-\frac{\alpha_c F}{RT} \left(\Phi_1 - \Phi_2 - U_0^{HOR} \right) \right) \right] \quad (19)$$

$$i_{ORR_{4e^-}} = -i_{0_{ORR_{4e^-}}} \frac{p_{O_2}}{p_{O_2}^{ref}} \left(\frac{a_{HM}}{a_{HM}^{ref}} \right)^4 \exp\left(-\frac{\alpha_c F}{RT} \left(\Phi_1 - \Phi_2 - U_0^{ORR_{4e^-}} \right) \right) \quad (20)$$

$$i_{ORR_{2e^-}} = -i_{0_{ORR_{2e^-}}} \frac{p_{O_2}}{p_{O_2}^{ref}} \left(\frac{a_{HM}}{a_{HM}^{ref}} \right)^2 \exp\left(-\frac{\alpha_c F}{RT} \left(\Phi_1 - \Phi_2 - U_0^{ORR_{2e^-}} \right) \right) \quad (21)$$

Where $i_{0,HOR}$, $i_{0,ORR_{4e^-}}$, and $i_{0,ORR_{2e^-}}$ are the respective exchange current densities, α_a and α_c are the anode and cathode coefficients, U_0^{HOR}, $U_0^{ORR_{4e^-}}$, and $U_0^{ORR_{2e^-}}$ are the respective standard potentials, p_i and p_i^{ref} are the partial pressure and reference pressure of species i, and a_{HM} and a_{HM}^{ref} are the proton activity and reference proton activity, respectively, R is the ideal gas constant, and T is the absolute temperature [24]. Kinetic properties used in the model are listed in table 2. The proton activity is taken to be the fraction of membrane sulfonic-acid sites that are occupied by protons. The reference value for proton activity is that of protons in unexchanged Nafion and is taken to be equal to 1. The ratio a_{HM}/a_{HM}^{ref} reduces to the mole fraction of protons occupying sulfonic acid sites, which is equivalent to $1 - f_{Ce}$.

2.3 Chemical degradation and mitigation kinetics

The modeling approach for the degradation of Nafion is based on the works of Wong and Kjeang and the reactions are listed in table 3 [32, 42]. Figure 4 illustrates the different types of degradation of Nafion when

Table 2. Kinetic properties.

Property		Units	HOR [30]	$4e^-$ ORR [30]	$2e^-$ ORR
Activation energy	E_A	J mol^{-1}	9500	73 269	—
Exchange current density	i_0	A cm^{-2}	$10^{-4}\left(\frac{E_A}{R}\left(\frac{1}{T}-\frac{1}{T_{ref}}\right)\right)$	$1.1\times10^{-8}\left(\frac{E_A}{R}\left(\frac{1}{T}-\frac{1}{T_{ref}}\right)\right)$	7×10^{-7}
Equilibrium potential	U_0	V	0	$4.1868((70650+8T\log T-92.4\,T)/2\,F)$	0.695
Anodic transfer coefficient	α_a		1	—	—
Cathodic transfer coefficient	α_c		1	1	1
Thiele mass transport coefficient	ϕ_{mt}	$\frac{\text{bar}\cdot\text{cm}\cdot\text{s}}{\text{mol}}$	8000	6000	$E=1$

Table 3. Membrane degradation reaction kinetics.

Reaction Number		Rate constant	Ref.
1	$H_2O_2 \rightarrow 2HO^\bullet$	$3\times10^{-3}\,\text{s}^{-1}$	fit
2	$R_fSO_3 + HO^\bullet \rightarrow R_f\alpha O^\bullet + 4HF$	$3.7\times10^6\,\text{M}^{-1}\text{s}^{-1}$	[32, 42]
3	$R_f\alpha O^\bullet + 3HO^\bullet \rightarrow R_f\beta O^\bullet + 6HF$	$3.75\times10^7\,\text{M}^{-1}\text{s}^{-1}$	[32, 42]
4	$R_f\beta O^\bullet + 2H_2O + HO^\bullet \rightarrow 2R_fCOOH + 3HF$	$7.5\times10^7\,\text{M}^{-1}\text{s}^{-1}$	[42]
5	$R_fCOOH + 2HO^\bullet \rightarrow R_fCF_2 + 2HF$	$5.8\times10^6\,\text{M}^{-1}\text{s}^{-1}$	[32, 42]
6	$Ce^{3+} + HO^\bullet + H^+ \rightarrow Ce^{4+} + H_2O_2$	$1\times10^{11}\,\text{M}^{-1}\text{s}^{-1}$	fit

attacked by hydroxyl radicals. All the reactions are assumed to be elementary steps, so that the reaction rates can be written as

$$r_h = k_h \sum_{i=1}^{n_h} c_i^{\nu_i} \tag{22}$$

where r_h, k_h, and n_h are the reaction rate, rate constant, and total number of reactants of reaction h, respectively, and c_i and ν_i are the concentration and stoichiometric coefficient of species i, respectively. The initial concentration of sulfonic-acid sites in the PEM is assumed to be equal to ρ_M/EW.

The degradation process can be initialized by reaction of hydroxyl ions at the side-chain or the end-chain. Once the initial attack of hydroxyl ion on the side chain has occurred, leading to the degradation of the sulfonic-acid site, the remaining CF_2 groups in the side chain will also degrade until the main chain is reached and attacked. The kinetic equations are simplified in order to account for the total number of sulfonic-acid groups, end-chain groups, and fluoride ions that are present in the Nafion membrane and are released as a result of chemical degradation. The amount of fluoride ions that exits the PEMFC, called the fluoride release rate (FRR), is a measurement often used to quantify chemical degradation. In the model, the FRR is calculated as the sum of hydrogen-fluoride fluxes at the gas channels.

The gas crossover rate through the membrane drives chemical degradation, as hydrogen and oxygen react to form hydrogen peroxide and hydroxyl radicals. The gas crossover rate rates are calculated as

$$\mathbf{N}_i = -\psi_i \nabla p_i \tag{23}$$

Where ψ_i and p_i are the permeation coefficient and partial pressure of species i, respectively. The initial values for the membrane permeation coefficients for hydrogen and oxygen are,

$$\psi_{H_{2,0}} = \left(2.2\times10^{-11}\phi_w + 2.9\times10^{-12}\right) \times \exp\left(\frac{21000}{R}\left(\frac{1}{T_{ref}}-\frac{1}{T}\right)\right) \tag{24}$$

$$\psi_{O_{2,0}} = \left(1.9\times10^{-11}\phi_w + 1.1\times10^{-12}\right) \exp\left(\frac{22000}{R}\left(\frac{1}{T_{ref}}-\frac{1}{T}\right)\right) \tag{25}$$

Where ϕ_w is the volume fraction of water, T_{ref} is the reference temperature (303.15 K) [43].

To account for the impact of membrane degradation on gas crossover, a polynomial function was fit to the data of Coms *et al* [18]. The modified permeation coefficients are,

$$\psi_i = \left(102\left(\frac{c_{R_fSO_3}}{\frac{\rho_M}{EW}}\right)^2 - 201\left(\frac{c_{R_fSO_3}}{\frac{\rho_M}{EW}}\right) + 100\right)\psi_{i,0} \tag{26}$$

(a)

$$-[(CF_2-CF_2)_x-(CF-CF_2)]-CO_2H + 2\,HO^\bullet \rightarrow -[(CF_2-CF_2)_x-(CF)]-CO_2H + 2\,HF + CO_2$$

with side chain:
$$O - CF_2 - CF_3-CF - O - CF_2CF_2SO_3H$$

$$-[(CF_2-CF_2)_x-(CF-CF_2)]-CO_2H + 3\,HO^\bullet \rightarrow -[(CF_2-CF_2)_x-(CF-CF_2)]-CO_2H + 6\,HF + \text{byproducts}$$

$R_f\alpha O^\bullet$ $R_f\beta O^\bullet$

(b)

$$-[(CF_2-CF_2)_x-(CF-CF_2)]-CO_2H + 2\,H_2O + HO^\bullet \rightarrow 2\ -[(CF_2-CF_2)_{x-1}]-CF_2-CO_2H + 3\,HF$$

$R_f\beta O^\bullet$

(c)

$$-[(CF_2-CF_2)_x-(CF-CF_2)]-CO_2H + 2\,HO^\bullet \rightarrow -[(CF_2-CF_2)_x-(CF)]-CO_2H + 2\,HF + CO_2$$

with side chain:
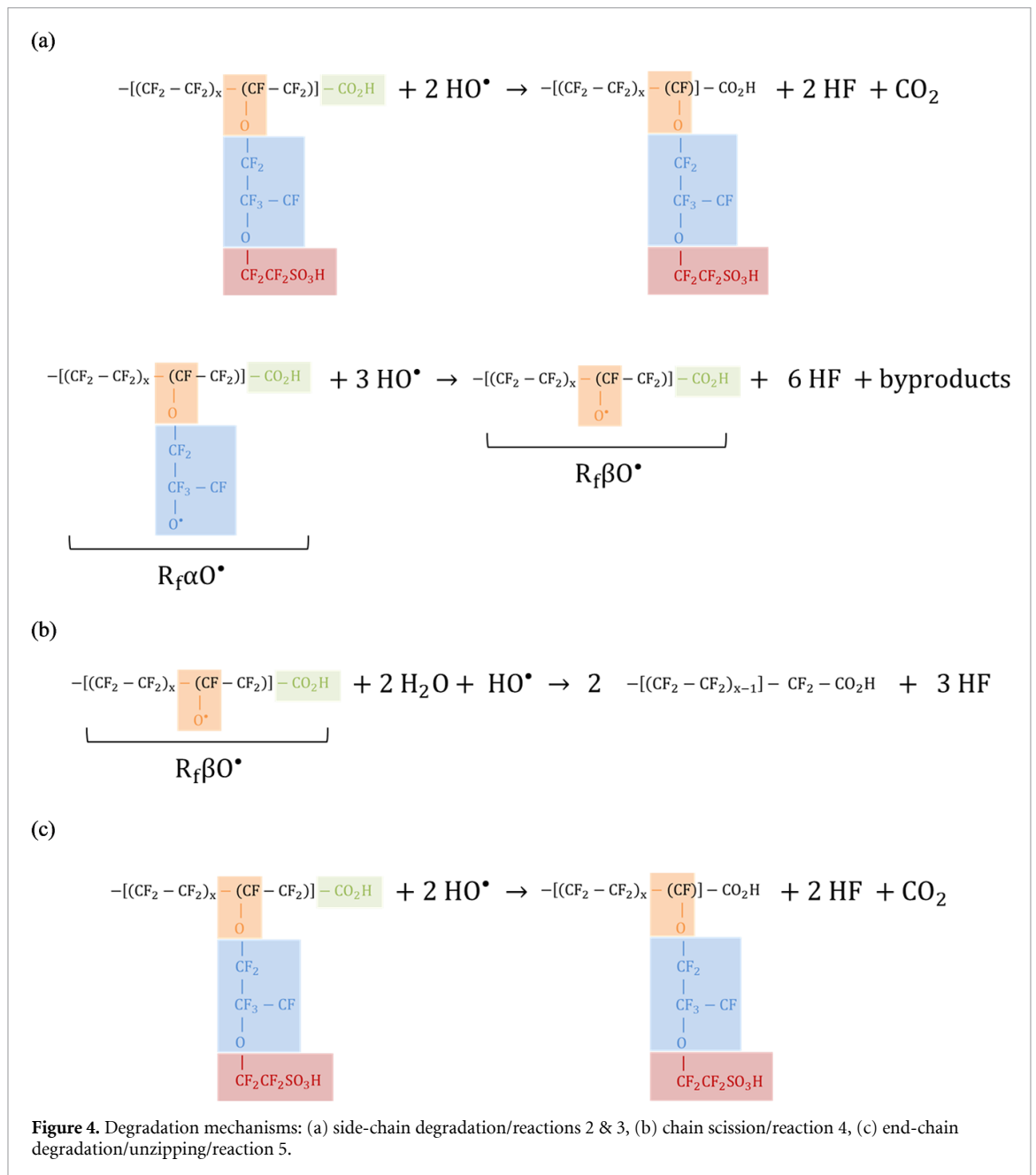$$O - CF_2 - CF_3-CF - O - CF_2CF_2SO_3H$$

Figure 4. Degradation mechanisms: (a) side-chain degradation/reactions 2 & 3, (b) chain scission/reaction 4, (c) end-chain degradation/unzipping/reaction 5.

Where $c_{R_fSO_3}$ the concentration of sulfonic-acid sites in the membrane. The experimental data used for fitting is shown in figure S1 of the supplemental Material.

The degradation products H_2O_2 and HF are generated in the catalyst layers and membrane and are allowed to diffuse into to the GDLs and out of the PEMFC. The rate of diffusion for these species is calculated using Fick's law. Due to the short lifetime of the radical species, the diffusion distance can be approximated as zero [22, 31] Furthermore, it is assumed that the concentration of Ce^{4+} is negligible, as it has been shown that over 99% of cerium ions are in the 3 + charge state during cell operation [27, 44]. Previous studies on modeling mitigation of chemical degradation in PEMFCs using cerium have incorporated the presence of iron-ion contaminants leading to generation of peroxide radicals via Fenton's reaction [25, 27, 31, 32, 42]. Incorporation of iron-ion contaminant effects could be included in the model by further modifying the concentrated-solution-theory equations to include additional terms in the transport equations and by including the relevant chemical reactions in the chemical-degradation model. In this study it is assumed that hydrogen peroxide degrades into peroxide radicals at a constant rate and does not consider the influence of iron ions. The primary source of iron ions in the membrane is due to migration from metallic bipolar plates [12] A graphite flow field was used in the experiment whose data was used to fit the model, so the amount of iron in the membrane can be assumed to be neglegible [18].

2.4 Model solution

The model is run in MATLAB. To initialize the simulation, certain operating parameters such as temperature, pressure, feed stoichiometry, air stoichiometry, membrane properties, initial cerium doping, *etc* must be specified. These parameters are used to calculate the initial condition for the transient simulation by solving the PEMFC model under steady-state conditions. Furthermore, the cerium is assumed to be present in the membrane only at uniform concentration, and the initial cerium flux is zero. The governing equations are constructed using a finite-volume method approach, which enforces conservation of mass and energy. The system of equations is solved using a multidimensional Newton-Raphson technique (Band(j)) developed by Newman [35, 45], which is detailed in appendix C of Newman and Thomas-Alyea [35]. Each domain in the model is discretized using 40 mesh points. The full list of equations and boundary conditions are listed in table S2 in the Supplemental Material. The simulation must be initialized by specifying certain conditions, including: cell current or cell voltage, relative humidity in the hydrogen and air feeds, stoichiometry of feed or feed rates, temperature, pressure in the gas channels, membrane thickness, and cerium content (f_{Ce}), To incorporate transient effects, a Crank-Nicolson approach was used to calculate the time derivatives in the mass- and energy-balance equations.

To explore the impact of the various contribution to the overpotentials, a voltage-loss breakdown was calculated by removing limiting factors to PEMFC performance sequentially from the final polarization curve. The transport losses attributed to cerium are divided into two categories. The first is effects that the cerium ions have in changing the transport properties of water and protons. The second is losses that occur due to the reduction in proton activity in the membrane phase, which is included in the kinetics in equations (19, 20 and 21). To remove this limitation, we set the ratio $a_{HM}/a_{HM}^{ref} = 1$, which assumes a membrane with zero cerium content. Mass-transport limitations occur when the PEMFC starts to become reactant limited. To remove mass-transport limitations, the simulation is run at a high stoichiometry for hydrogen gas and air. The ohmic losses are due to resistance through each of the PEMFC layers; the ohmic losses are removed by setting a high value for conductivity both in the membrane phase and solid phase. Kinetic losses occur due to the activation energy required for the electrochemical reactions. As a PEMFC operates, crossover gasses will permeate the membrane and react at the electrodes, leading to a mixed potential at the electrodes and an overall decrease in cell potential. The gas crossover effects lead to the difference between the thermodynamic potential and the open-circuit voltage. The thermodynamic potential, which is the maximum possible potential that can be achieved, is taken to be 1.18 A cm^{-2} for the oxygen reduction reaction at 80 °C.

3 Results and discussion

3.1 Comparison of dilute and concentrated-solution theory

To illustrate the effects and needs for concentrated-solution theory, a comparison is made with a dilute-solution theory model using Nernst-Planck equation (27) for cerium. The proton flux and water flux were calculated using equations (13) and (15), where the $\nabla \mu_{Ce,H}$ terms are assumed to be zero. The diffusion and migration coefficients for cerium in Nafion as a function of water content are taken from Baker *et al* [44].
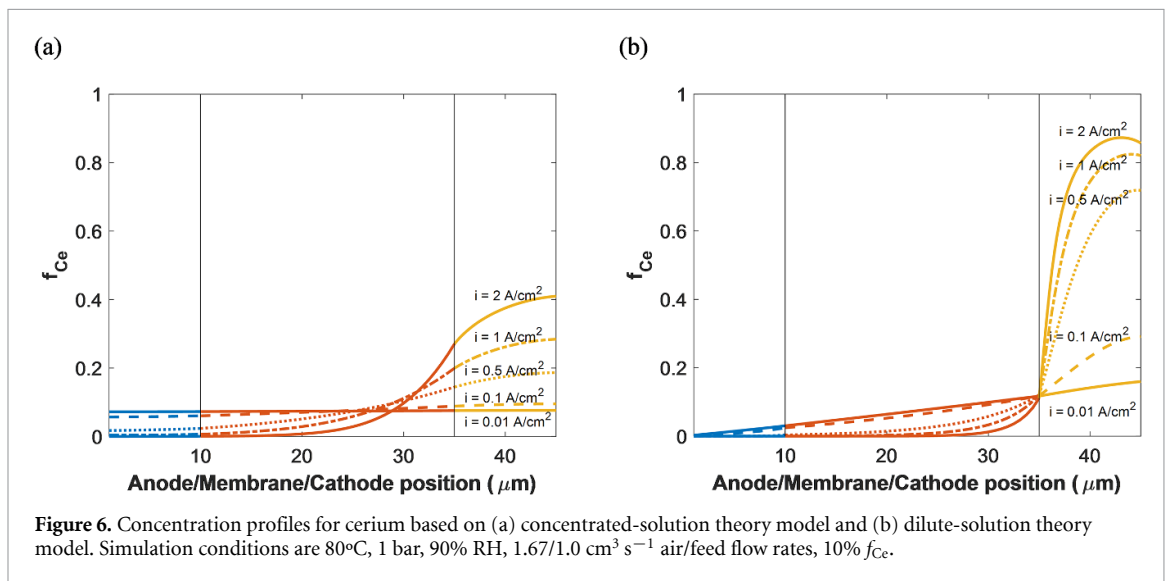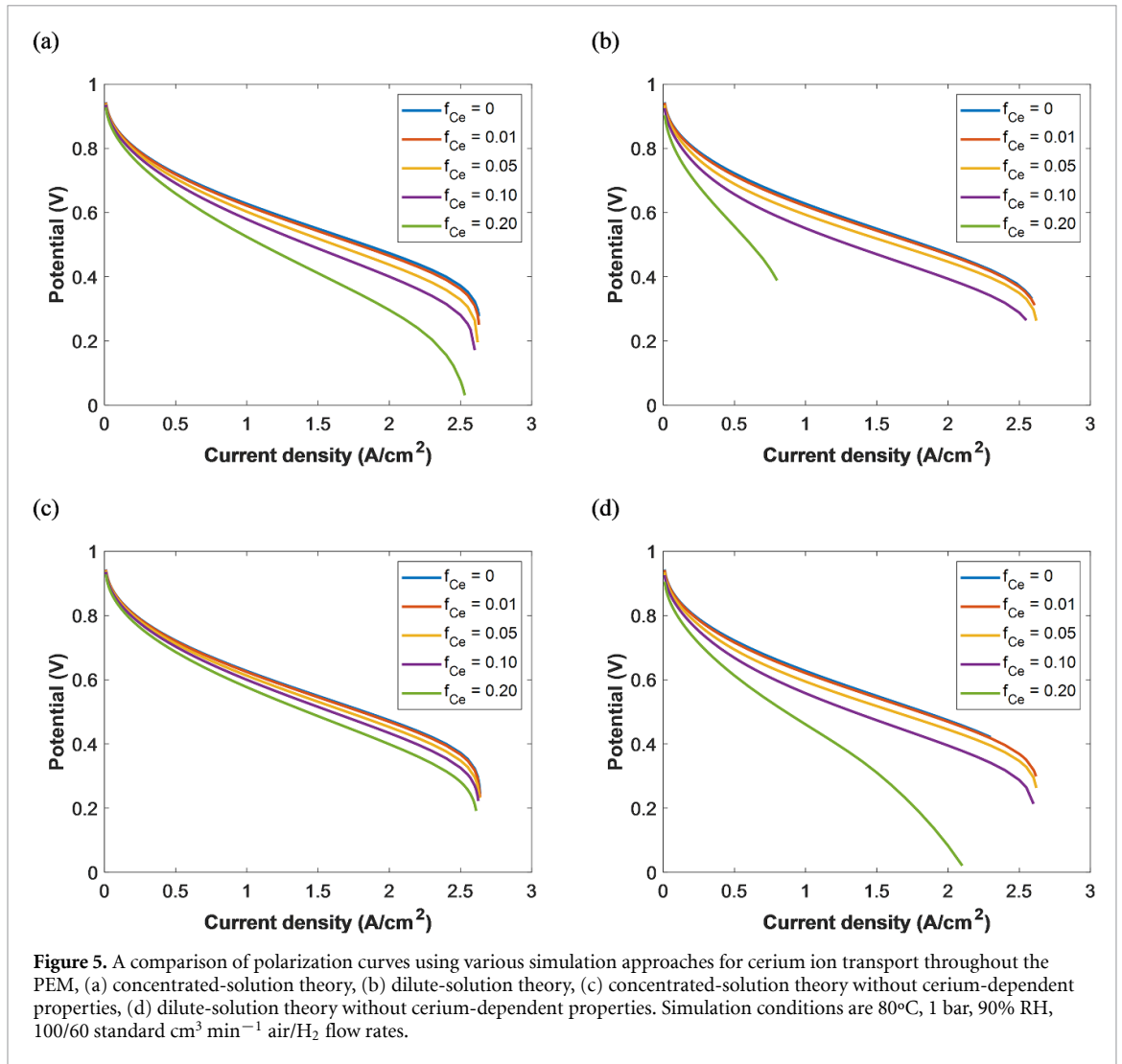
$$\mathbf{N}_{Ce} = -z_{Ce}u_{Ce}c_{Ce}F\nabla\Phi - \mathcal{D}_{Ce}\nabla c_{Ce} \tag{27}$$

Where $\mathcal{D}_{Ce}(\lambda) = 3.11 \times 10^{-8}\lambda$ cm^2 s^{-1} and $u_{Ce}(\lambda) = 1.89 \times 10^{-6}\lambda$ cm^2 V^{-1} s^{-1}.
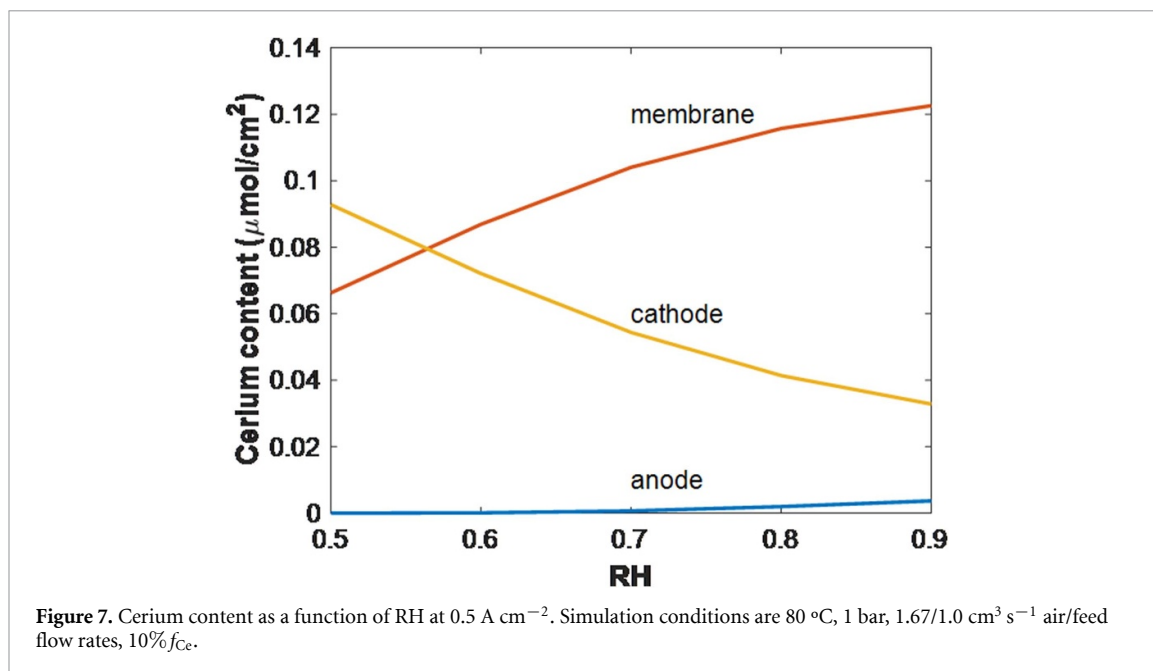
The dilute-solution theory model includes all of the chemical degradation reactions in table 3 as well as the cerium effects on hydrogen activity. Polarization curves generated from the concentrated-solution-theory model and dilute-solution-theory model are shown in figures 5(a) and (b).

As expected, the two models exhibit good agreement at low cerium concentrations. However, at higher cerium concentrations, the dilute-solution-theory model reaches mass-transport limitations at lower current densities as the cathode catalyst layer becomes saturated with cerium ions. The cerium content profiles in figure 6 clearly show that as the current density increases, the potential gradient increases and the migration term drives cerium ions into the cathode catalyst layer. However, the migration term dominates the transport of cerium in the dilute-solution-theory model. Even at a low current density value of 0.01 A cm^{-2}, a concentration gradient of cerium across the PEMFC is predicted by the dilute-solution-theory model. In contrast, the concentrated-solution-theory model predicts a uniform distribution of cerium across the cell at 0.01 A cm^{-2}. Therefore, the dilute-solution-theory model tends to overestimate the migration term. The concentrated-solution-theory model corrects this term by including the solvent-ion interactions between the cerium ions and water, which drives cerium ions back toward the membrane and anode catalyst layer.

To analyze the impact of cerium on transport of water and protons through the membrane, both models are modified so that the transport properties (i.e. ξ, κ, $t_{Ce^{3+}}$, α_{ij}'s) are calculated for a membrane with zero

Figure 5. A comparison of polarization curves using various simulation approaches for cerium ion transport throughout the PEM, (a) concentrated-solution theory, (b) dilute-solution theory, (c) concentrated-solution theory without cerium-dependent properties, (d) dilute-solution theory without cerium-dependent properties. Simulation conditions are 80°C, 1 bar, 90% RH, 100/60 standard cm^3 min^{-1} air/H$_2$ flow rates.

Figure 6. Concentration profiles for cerium based on (a) concentrated-solution theory model and (b) dilute-solution theory model. Simulation conditions are 80°C, 1 bar, 90% RH, 1.67/1.0 cm^3 s^{-1} air/feed flow rates, 10% f_{Ce}.

cerium content. These polarization curves are shown in figures 5(c) and (d). The difference in the results in figures 5(a) and (c) show that accounting for the amount of cerium in determining membrane transport properties has a significant effect in the concentrated-solution-theory model. The inclusion of cerium dependence leads to higher ohmic losses, as conductivity decreases with cerium content (see figure 2). The limiting current density converges to the same value when the cerium effects on membrane transport

Figure 7. Cerium content as a function of RH at 0.5 A cm^{-2}. Simulation conditions are 80 °C, 1 bar, 1.67/1.0 cm^3 s^{-1} air/feed flow rates, 10% f_{Ce}.

properties are not considered; therefore, the increase in mass-transport limitations with cerium content can be attributed to the cerium effects on transport properties and not on the loss of proton activity caused by the presence of cerium ions. A comparison between the results in figures 5(b) and (d) show the impact of cerium-ion effects on transport properties in the dilute-solution-theory model. There is little difference between the polarization curves at low cerium content due to the dominance of the cerium migration in comparison to the diffusion term. The limiting current density decreases with cerium content in both cases, with a steeper drop-off for the limiting current density when the cerium-dependent transport properties are used.

Figure 7 shows the dependence of cerium concentration throughout the cell on RH using the concentrated-solution-theory model. Increasing the RH into the cell drives the cerium ions back toward the anode catalyst layer and leads to better retention of cerium ions in the membrane, while decreasing the RH leads to accumulation of cerium in the cathode catalyst layer.
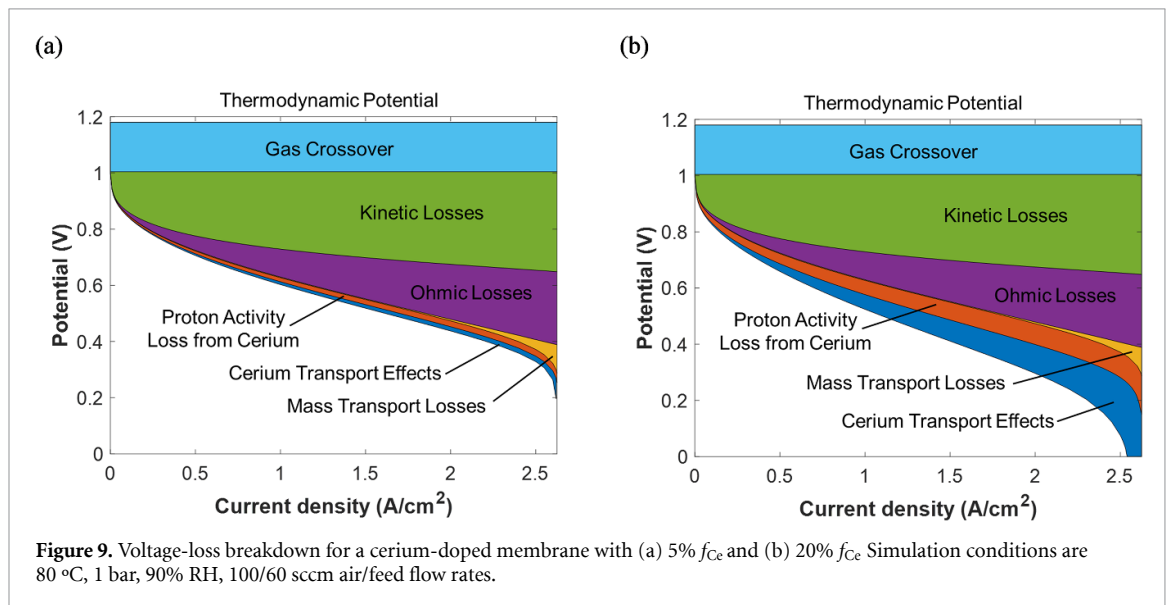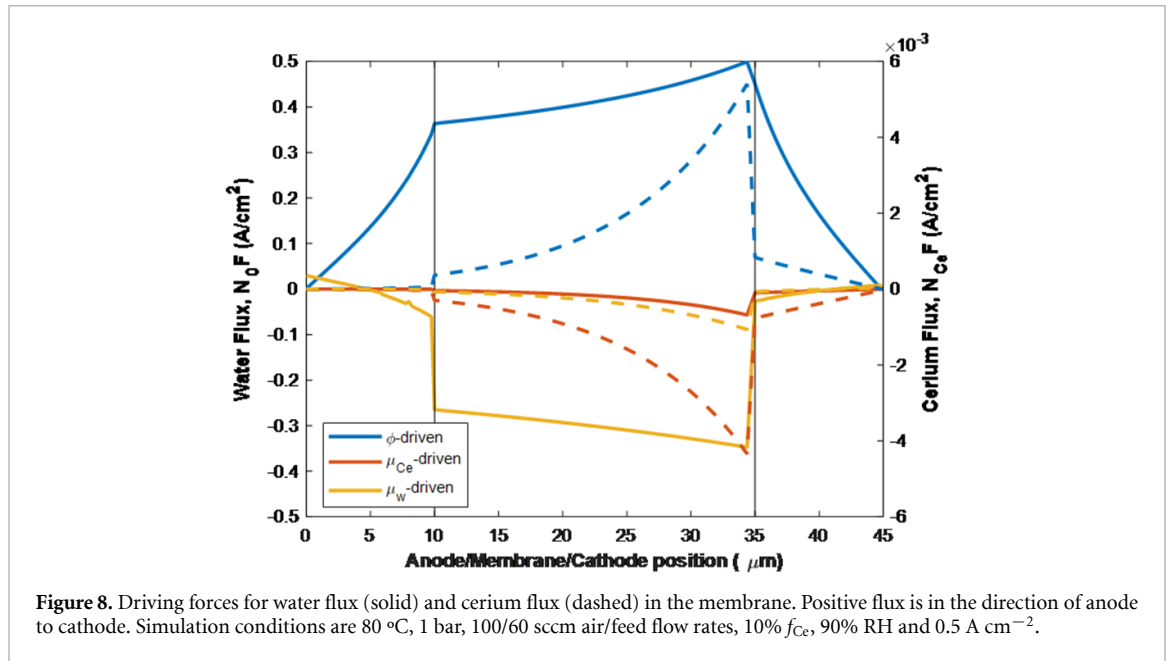
The results in figure 8 provide a breakdown of the various driving forces for transport of water and cerium throughout the membrane. For both species, the migration term is positive, which means that the electrostatic forces are driving them from anode to cathode. At steady state, the migration term is balanced by the cerium and water electrochemical potential terms. The μ_{Ce}-driven term in the cerium flux increases in an exponential manner across the membrane, whereas the μ_w term in the water flux is roughly linear across the membrane. Thus, the primary driving force for the cerium ions entering the cathode is due to the Φ contribution to the overall flux, and the μ_{Ce} contribution drives cerium back toward the membrane and anode.

3.2 Voltage-loss breakdown

To analyze the performance losses from the addition of cerium to the membrane, a voltage loss breakdown curves was carried out for 5% f_{Ce} and 20% f_{Ce} in the membrane. The results in figure 9 show that at low cerium content, below 5% f_{Ce}, the performance losses from the addition of cerium are small compared to the kinetic and ohmic losses. As the cerium content increases, the voltage losses increase and become one of the primary sources of performance losses. The impact of cerium ions on mass-transport properties leads to the decrease in limiting current density in the PEMFC, whereas the presence of cerium ions in the membrane limiting access to catalyst sites contributes to ohmic losses. Both proton activity loss from cerium and cerium transport effects have significant contributions to the voltage loss breakdown, further showing the benefits of using a concentrated-solution-theory approach.
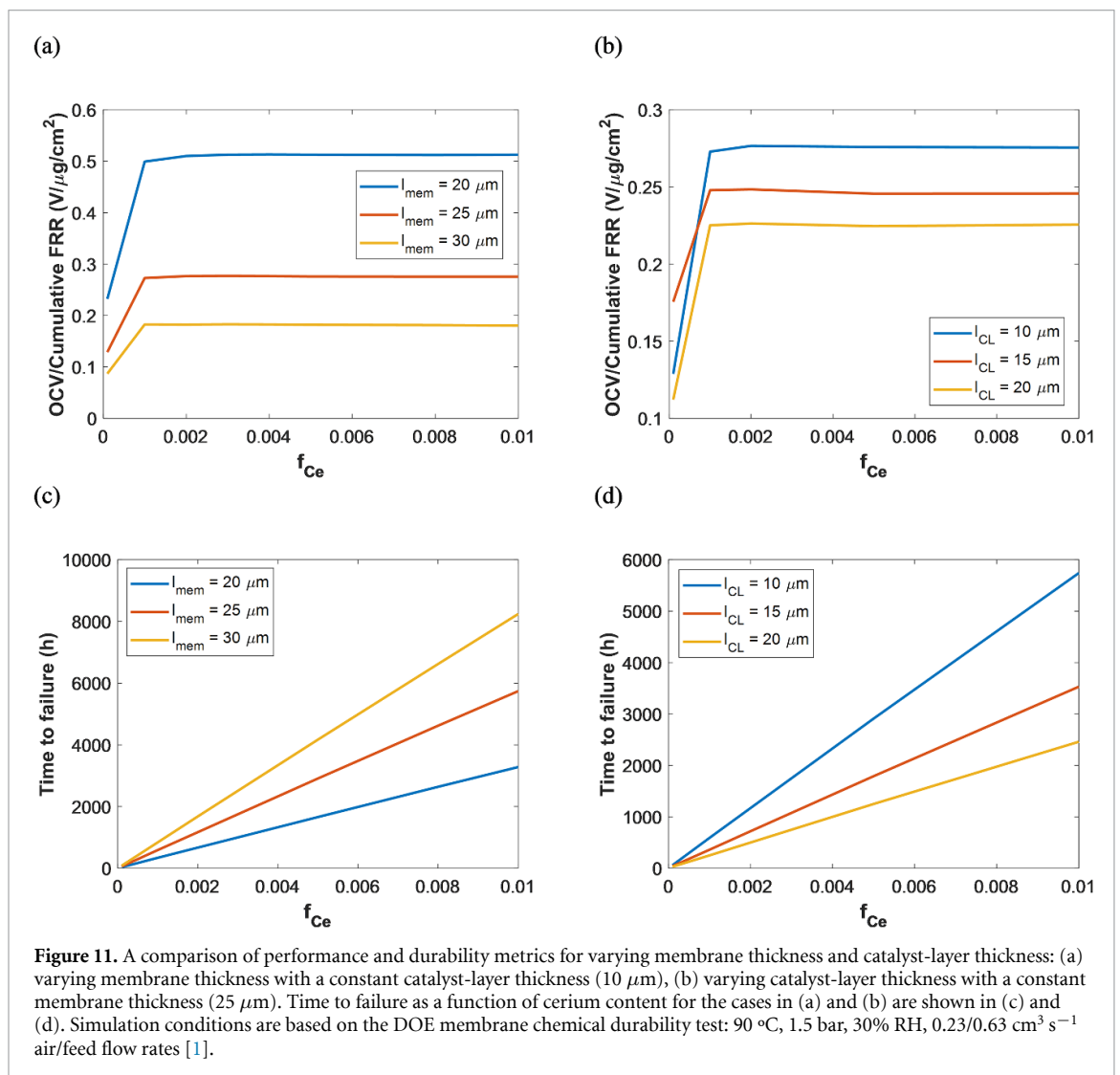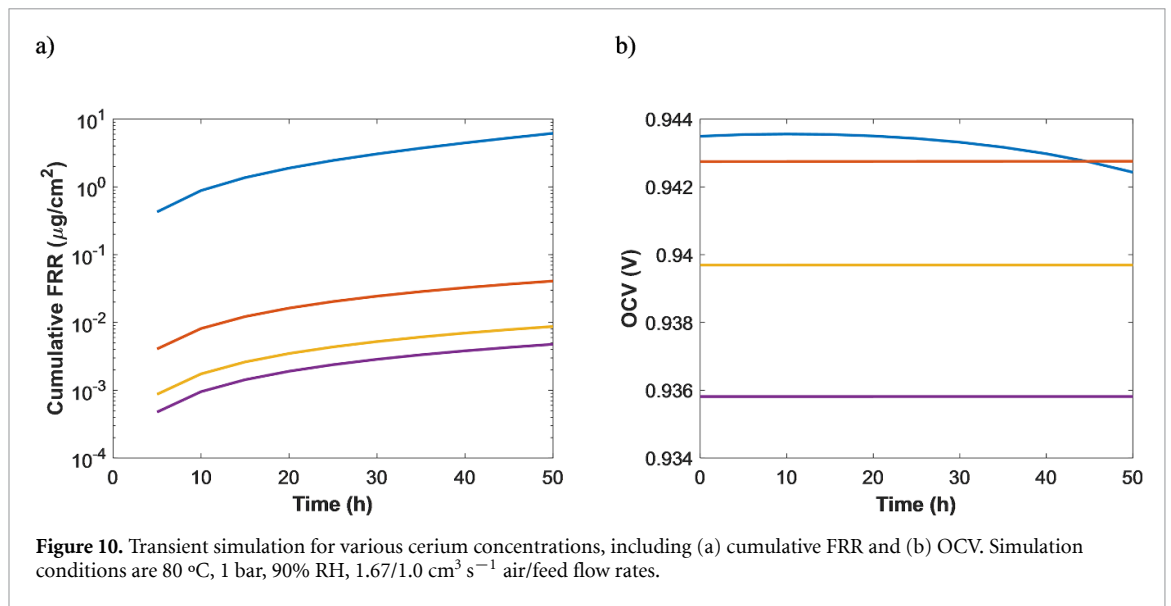
3.3 Cerium impacts on durability and performance

To look at the impact of cerium on degradation rate, several transient simulations were run at a constant current density. The results shown in figure 10 show the effectiveness of adding cerium to the membrane to reducing FRR. Between 0% cerium content and 1% cerium content, the cumulative FRR decreases by two orders of magnitude. The FRR decreases further as more cerium is added, however the mitigation rate

Figure 8. Driving forces for water flux (solid) and cerium flux (dashed) in the membrane. Positive flux is in the direction of anode to cathode. Simulation conditions are 80 $^{\circ}$C, 1 bar, 100/60 sccm air/feed flow rates, 10% f_{Ce}, 90% RH and 0.5 A cm^{-2}.

Figure 9. Voltage-loss breakdown for a cerium-doped membrane with (a) 5% f_{Ce} and (b) 20% f_{Ce} Simulation conditions are 80 $^{\circ}$C, 1 bar, 90% RH, 100/60 sccm air/feed flow rates.

decreases; thereby suggesting that only minimal cerium is required. However, in full cells multidimensional aspects and eventually cerium removal or interactions within the electrodes probably mean the values here are lower than in reality. While the cerium decreases the rate of chemical degradation in the membrane, the open circuit voltage (OCV) also decreases. The OCV is highest at 0% cerium and decreases as more cerium is added to the membrane. However, the OCV decays over time when zero cerium is present in the membrane; in all cases with cerium, the OCV decay is negligible.

Performance and durability are often seen as competitive metrics; increasing membrane thickness is a strategy used to improve durability in commercial PEMFC vehicles, while decreasing membrane thickness is often the focus of research due to less material use, better water management and less ohmic drop, and thus a higher performance. Likewise, catalyst loading and subsequently catalyst layer thickness is a critical design variable. A sensitivity study was carried out to study the effects of membrane thickness and catalyst layer thickness on performance and durability as a function of cerium content. As was established by the results in figure 10, the majority of the mitigation benefits occur with a cerium content of $f_{Ce} \leqslant 1\%$ in the membrane. The results in figure 11 show the ratio of OCV to FRR for different membrane and catalyst-layer thicknesses and the respective times to failure, which is defined as a hydrogen crossover current density of >2 mA cm^{-2} [1]. The results in figures 11(a) and (b) shows that the tradeoff between performance losses and degradation mitigation levels off very quickly, as the mitigation benefits increase quickly at small amounts of cerium and then begin to asymptote, whereas the OCV decrease with cerium content is more linear. The time to failure

Figure 10. Transient simulation for various cerium concentrations, including (a) cumulative FRR and (b) OCV. Simulation conditions are 80 °C, 1 bar, 90% RH, 1.67/1.0 cm^3 s^{-1} air/feed flow rates.

Figure 11. A comparison of performance and durability metrics for varying membrane thickness and catalyst-layer thickness: (a) varying membrane thickness with a constant catalyst-layer thickness (10 μm), (b) varying catalyst-layer thickness with a constant membrane thickness (25 μm). Time to failure as a function of cerium content for the cases in (a) and (b) are shown in (c) and (d). Simulation conditions are based on the DOE membrane chemical durability test: 90 °C, 1.5 bar, 30% RH, 0.23/0.63 cm^3 s^{-1} air/feed flow rates [1].

increases linearly with cerium content for all cases and increases with increasing membrane thickness and decreases with increasing catalyst-layer thickness. The thicker membranes increase lifetime because the crossover gases are slower to permeate the membrane, while the thicker catalyst layers decrease lifetime due to the increased reaction rate due to a greater availability of reaction sites for radical formation. These results

show that an optimal tradeoff between performance and durability requires (within reason) thicker membranes and thinner catalyst layers, while also considering limitations due to local losses and flooding that are not included in this model.

4. Conclusions

A full-cell, transient durability model with a microkinetic framework for degradation and concentrated-solution-theory based transport and mitigating effects of cerium ion was developed for a proton-exchange-membrane fuel cell. The model predicted the migration of cerium out of the membrane into the catalyst layers, with the cerium primarily accumulating in the cathode. Simulation results agree with decrease in FRR and OCV drop as the cerium concentration increases. A comparison of results between dilute-solution-theory and concentrated-solution-theory shows that the dilute-solution-theory overestimates the migration force acting on cerium, which leads to an accumulation of cerium ions in the cathode catalyst layer and subsequent steep drop in limiting current densities at high cerium content. A voltage-loss breakdown shows that cerium leads to voltage losses in the cell due to both proton activity loss and modification of membrane transport properties, and these losses occur simultaneously and are comparable in magnitude. The concentrated-solution-theory model corrects for this effect by accounting for the interaction between cerium ions and water in the membrane. Transient simulation results show that the majority of the benefits to chemical degradation mitigation can be achieved at <1% cerium content in the membrane (with the assumed 1-D, single-phase model), at which point the decrease in performance is largely outweighed by the degradation mitigation increase. Additional analysis shows that the time to failure is roughly linear with cerium content at low cerium content, where the slope is dependent on the membrane and catalyst-layer thicknesses. While optimizing performance and durability, thicker membranes and thinner catalyst layers should be considered which are considered within reasonable design limitations. Extensions to the model include incorporation of metal ions and radical generation via Fenton's reaction and explicit consideration of cerium ions in the 4+ charge state in the concentrated-solution-theory equations, as well as the addition of multiphase phenomena for modeling higher relative-humidity conditions. The model could also be modified to include higher dimensional effects such as along-the-channel or land/channel distribution of cerium.

Acknowledgments

ORCID iDs

Victoria M Ehlinger ⬤ https://orcid.org/0000-0001-7333-1271
Andrew R Crothers ⬤ https://orcid.org/0000-0003-4466-1057
Ahmet Kusoglu ⬤ https://orcid.org/0000-0002-2761-1050
Adam Z Weber ⬤ https://orcid.org/0000-0002-7749-1624

References

[1] Gittleman C S, Coms F D and Lai Y H 2012 *Polymer Electrolyte Fuel Cell Degradation*, eds M M Mench, E C Kumbur and T N Veziroglu (Waltham, MA: Academic) pp 15
[2] Kusoglu A and Weber A Z 2015 *J. Phys. Chem. Lett.* **6** 4547
[3] Kreitmeier S, Lerch P, Wokaun A and Buchi F N 2013 *J. Electrochem. Soc.* **160** F456
[4] Mukundan R, Baker A M, Kusoglu A, Beattie P, Knights S, Weber A Z and Borup R L 2018 *J. Electrochem. Soc.* **165** F3085
[5] Lai Y H, Rahmoeller K M, Hurst J H, Kukreja R S, Atwan M, Maslyn A J and Gittleman C S 2018 *J. Electrochem. Soc.* **165** F3217
[6] Lin R, Gulzow E, Schulze M and Friedrich K A 2011 *J. Electrochem. Soc.* **158** B11
[7] Liu D and Case S 2006 *J. Power Sour.* **162** 521
[8] Dubau L *et al* 2014 *Wiley Interdiscip. Rev. Energy Environ.* **3** 540
[9] Zaton M, Roziere J and Jones D J 2017 *Sustain. Energy Fuels* **1** 409
[10] Coms F D 2008 *ECS Trans.* **16** 235
[11] Kinumoto T, Inaba M, Nakayama Y, Ogata K, Umebayashi R, Tasaka A, Iriyama Y, Abe T and Ogumi Z 2006 *J. Power Sour.* **158** 1222
[12] Pozio A, Silva R F, Francesco M D and Giorgi L 2003 *Electrochim. Acta* **48** 1543
[13] Kusoglu A, Karlsson A M, Santare M H, Cleghorn S and Johnson W B 2006 *J. Power Sour.* **161** 987
[14] Kusoglu A, Karlsson A M, Santare M H, Cleghorn S and Johnson W B 2007 *J. Power Sour.* **170** 345
[15] Uchiyama T, Kato M, Ikogi Y and Yoshida T 2012 *J. Fuel Cell Sci. Technol.* **9** 061005
[16] Kusoglu A, Santare M H and Karlsson A M 2011 *J. Polym. Sci.* B **49** 1506

[17] Ding G, Santare M H, Karlsson A M and Kusoglu A 2016 *J. Power Sour.* **216** 114
[18] Coms F D, Liu H and Owejan J E 2008 *ECS Trans.* **16** 1735
[19] Trogadas P, Parrondo J and Ramani V 2008 *Electrochem. Solid State Lett.* **11** B113
[20] Trogadas P, Parrondo J and Ramani V 2012 *ACS Appl. Mater. Interfaces* **4** 5098
[21] Stewart S M, Spernjak D, Borup R, Datye A and Garzon F 2014 *ECS Electrochem. Lett.* **3** F19
[22] Coms F D, Schlick S and Danilczuk M 2018 *The Chemistry of Membranes Used in Fuel Cells: Degradation and Stabilization* 1st edn, ed S Schlick (Hoboken, NJ: Wiley)
[23] Zaton M, Prelot B, Donzel N, Roziere J and Jones D J 2018 *J. Electrochem. Soc.* **165** F3281
[24] Weber A Z and Delacourt C 2008 *Fuel Cells* **0** 459
[25] Wong K H and Kjeang E 2017 *J. Electrochem. Soc.* **164** F1179
[26] Wong K H and Kjeang E 2019 *J. Electrochem. Soc.* **166** F128
[27] Gubler L and Koppenol W H 2012 *J. Electrochem. Soc.* **159** B211
[28] Ehlinger V M, Kusoglu A and Weber A Z 2019 *J. Electrochem. Soc.* **166** F3255
[29] Weber A Z and Newman J 2004 *J. Electrochem. Soc.* **151** A326
[30] Weber A Z 2004 Modeling water management in polyer-electrolyte fuel cells *Dissertation* (Berkeley, CA: University of California)
[31] Gubler L, Dockheer S M and Koppenol W H 2011 *J. Electrochem. Soc.* **158** B755
[32] Wong K H and Kjeang E 2014 *J. Electrochem. Soc.* **161** F823
[33] Fuller T F 1992 *Solid-polymer-electrolyte Fuel Cells* (Berkeley, Ann Arbor: University of California) pp 254
[34] Fuller T F and Newman J 1992 *J. Electrochem. Soc.* **139** 1332
[35] Newman J and Thomas-Alyea K E 2004 *Electrochemical Systems* (Hoboken, NJ: John Wiley & Sons, Inc.)
[36] Monroe C W and Newman J 2006 *Ind. Eng. Chem. Res.* **45** 5361
[37] Delacourt C and Newman J 2008 *J. Electrochem. Soc.* **155** B1210
[38] Crothers A R, Darling R M, Kushner D I, Perry M L and Weber A Z 2020 *J. Electrochem. Soc.* **167** 013549
[39] Crothers A R, Darling R M, Kusoglu A, Radke C J and Weber A Z 2020 *J. Electrochem. Soc.* **167** 013548
[40] Baker A M, Crothers A R, Chintam K, Luo X, Weber A Z, Borup R L and Kusoglu A 2020 *ACS Appl. Polym. Mater.* **2** 3642–56
[41] Baker A M, Mukundan R, Spernjak D, Judge E J, Advani S G, Prasad A K and Borup R L 2016 *J. Electrochem. Soc.* **163** F1023
[42] Wong K H and Kjeang E 2015 *ChemSusChem* **8** 1072
[43] Weber A Z and Newman J 2004 *J. Electrochem. Soc.* **151** A311
[44] Baker A M, Babu S K, Mukudan R, Advani S G, Prasad A K, Spernjak D and Borup R L 2017 *J. Electrochem. Soc.* **164** F1272
[45] Newman J 1968 *Ind. Eng. Chem. Fundam.* **7** 514